| | |
|---|---|
| Title | Properties of porous AlN multilayered ceramic sandwich substrates |
| Author(s) | Boey, Freddy Yin Chiang; Tok, Alfred Iing Yoong; Long, Y.; Yeong, H. Y. |
| Citation | Boey, F. Y. C., Tok, A. I. Y., Long, Y., & Yeong.H. Y. (2002). Properties of porous AlN multilayered ceramic sandwich substrates. Journal of materials research, 17(5), 1061-1068. |
| Date | 2002 |
| URL | http://hdl.handle.net/10220/18840 |
| Rights |  |

# Properties of porous AlN multilayered ceramic sandwich substrates

F.Y.C. Boey, A.I.Y. Tok, Y. Long, and H.Y. Yeong
*School of Materials Engineering, Nanyang Technological University, Nanyang Avenue, Singapore 639798, Singapore*

(Received 24 July 2001; accepted 13 February 2002)

The development of denser and higher powered integrated circuits has led to a corresponding demand on the performance of dielectric substrates. This paper reports on the fabrication and properties of an AlN multilayered sandwich substrate comprising porous tape-cast layers sandwiched between nonporous layers. Tapes were produced by nonaqueous tape casting, with the porous tapes produced using polymer microspheres as sacrificial molds. Starting from initially $Al_2O_3$-rich tapes, the multilayered sandwich substrates were reaction sintered to produce AlN substrates. No interface cracking or delamination was observed in the substrates as a result of the processing. The added porosity resulted in a decrease in the substrate dielectric constant in correspondence to porosity volume. Mechanical strength of the sandwich substrates was improved over that of nonsandwich porous substrates, while substrates having noninterconnected pores showing higher mechanical strength than substrates with connected pores. Substrates with more than 2% porosity showed porosity-dependent thermal conductivity values, while thermal conductivity of substrates with less than 2% porosity was dependent on grain boundary effects. Thermal expansion coefficient of the substrates was unaffected by porosity levels.

## I. INTRODUCTION

Rapid progress made in the miniaturization of integrated circuit devices has led to the evolution of microelectronic circuitry with high device density. This trend of increasing device density has demanded stringent requirements on dielectric substrates. As predicted by the Semiconductor Industry Associate,[1] board-to-die frequency is expected to reach 1 GHz speed by the year 2007, while producing 200 W of power (Table I). As such, ceramic substrates have gained popularity in this area due to their good electrical insulation, high thermal conductivity, good mechanical support, and ability to operate at high temperatures without hazardous degradation in chemical, mechanical, or dielectric properties.[2,3]

Currently, aluminum oxide ($Al_2O_3$), glass, and glass–ceramics are utilized as substrate materials.[4] Although these materials generally provide adequate dielectric properties for current applications, they all possess the common disadvantage of a low thermal conductivity, about 15–37 W/mK for $Al_2O_3$. Recent attention has focused on aluminum nitride (AlN), as it does not have the inherent toxicity problems associated with BeO processing.[5,8] In addition to having a high thermal conductivity of about 320 W/mK, AlN has a relatively lower dielectric constant of 8, as compared to $Al_2O_3$ (10.5).[9,10] AlN also offers an excellent thermal expansion coefficient ($4.3 \times 10^{-6}$/°C) match to that of silicon ($3.9 \times 10^{-6}$/°C). Although the use of AlN offers superior thermal expansion coefficient and thermal properties, its material synthesis and production costs are very high.[11] AlN does not occur naturally and has to be synthesized from another starting material such as $Al_2O_3$.[6] As such, the cost of AlN powders is up to 10 times that of electronic grade $Al_2O_3$.[7] A novel reaction sintering method[12] was developed to overcome this. In this method, an initially $Al_2O_3$-rich substrate was reaction sintered at a relatively low temperature of 1680 °C in a carbothermal reduction furnace in a nitrogen atmosphere. This resulted in the concurrent densification and conversion of $Al_2O_3$ to AlN, achieving more than 98% densification and 94% AlN conversion. Formation of AlON was delayed until 1700 °C, at which a stoichiometric γ–AlON ($Al_2O_3N$) with a spinel type structure was obtained.[13]

TABLE I. Semiconductor Industry Associate (SIA) predicted trend.[1]

| Parameter | Year | |
|---|---|---|
| | 2001 | 2007 |
| Power | 40 (800 mm$^2$ die) | 200 (1250 mm$^2$ die) |
| I/O lines | 2000 | 5000 |
| Current to die | 18 A | 130 A |
| Board-to-die frequency | 250 MHz | 1 GHz |

  

Previous works[16] show that porous AlN dielectric substrates fabricated via the use of polymer microspheres as sacrificial molds successfully decreased substrate dielectric constant, as air has a dielectric constant of about 1.0. A linear relationship between substrate porosity and dielectric constant had been previously suggested.[14] This reduction in dielectric constant ($\epsilon$) can reduce the delay time of an electrical signal ($\tau$) by the following relationship,[15] where $c$ is the velocity of light:

$$\tau = \epsilon^{0.5}/c \quad . \tag{1}$$

The introduction of air as porosity within the ceramic substrate, however, reduced the substrate thermal conductivity and mechanical strength.

One method to overcome this would be the use of a sandwich structure[17–19] in the tape cast substrates. This would increase substrate strength and flexural rigidity and accord good dimensional stability, corrosion resistance, and improved fatigue properties to the substrate. The separation of high strength skins by a lightweight core carries most of the shear stresses.[20] In recent years, the extensive use of new materials has increased interest in sandwich structures. Of the various core materials used, closed-cell syntactic foams possess the greatest range for design flexibility. Depending on material type and fabrication process, mechanical properties can be tailored to meet specific requirements.[20] Another advantage of these structures is that the cores can protect the face against local buckling phenomena, preventing catastrophic failure.[21] Three-point bending studies of ceramic foams have been reported previously.[22]

This work focuses on the fabrication of an AlN multilayered sandwich substrate comprising porous tape-cast layers sandwiched between nonporous layers. Tapes were produced by nonaqueous tape casting, with the porous tapes produced via polymer microspheres as sacrificial molds. From initially $Al_2O_3$-rich tapes, the multilayered sandwich substrates were reaction sintered to produce AlN substrates.

## II. EXPERIMENTAL PROCEDURE

To study the effects of sandwich structure on the tape cast substrates, different sandwich structures were produced, with the level of porosity within the porous cores varied. The porous cores were fabricated via the addition of polymer microspheres into the tape casting slurry. Volumes of 5, 10, 15, and 20 vol% microspheres were added, and these microspheres were burnt off during the pyrolysis cycle, resulting in spherical noninterconnected pores. The skin of the sandwich structure was fabricated by tape casting without the addition of microspheres.

Formulation for the nonporous tapes (skin) comprised 75 wt% $Al_2O_3$ (Universal Photonics, Inc., NY), 20 wt% A1N (CERAC Specialty Inorganics, Milwaukee, WI), and 5 wt% $Y_2O_3$ (Merck, Darmstadt, Germany) as a sintering aid. The average particle size of $Al_2O_3$ and AlN particles was 1 $\mu$m. Porous tapes were fabricated with the same formulation, but with the addition of polymer microspheres.

The polymer microspheres were produced via spray drying, and the formulation and processing parameters were optimized previously.[23] Urea–formaldehyde resin (Aerolite FFD) (Ciba-Geigy, Basel, Switzerland) was added to cold water and mixed into a solution. A suitable hardener (Aerolite CB17) was then mixed into the solution. The solution was then stirred for 10 min using a magnetic stirrer and transferred over to a spray dryer to be spray dried. Solid polymer microspheres were chosen for the sacrificial cores as they had sufficient compressive strength (does not deform under ball milling and lamination), a low burnout temperature (ease of pyrolysis), and a $T_g$ above the lamination temperature (does not deform during lamination).

A spray dryer (Ohkawara LT-8) was used to produce the microspheres. The solution was fed into the spray dryer at 20 ml/min, and the inlet and outlet temperatures were set at 160 and 120 °C, respectively. Cyclone pressure was maintained at 200 mm of $H_2O$. Three different rotational speeds (15,000, 20,000, and 25,000 rpm) were used to produce microspheres of varying sizes. The microspheres were then sieved using 106, 75, 45, and 20 $\mu$m sieves to obtain sizes of 20–45, 45–75, and 75–106 $\mu$m.

The microspheres $T_g$ was determined to be approximately 103 °C using differential scanning calorimetry (Perkin-Elmer DSC7, CT) in a nitrogen atmosphere. Pyrolysis temperature of the microspheres was determined using thermogravimetric analysis (Perkin-Elmer TGA7) in an air atmosphere. From TGA results, the pyrolysis of the microspheres started at 240 °C when the polymer converted to carbon and was complete at about 700 °C. Characterization of the microspheres particle size and distribution was performed using particle analysis (Fritsch Particle Analysette 22). The $Al_2O_3$, AlN, and $Y_2O_3$ powders together with the microspheres were mixed in a horizontal ball mill for 24 h at 60 rpm using a corundum milling jar and high-purity alumina balls. The ball to weight ratio was 15:1. After ball milling, the powders were processed to form a slurry and tape cast on a batch process type caster. Optimization of tape casting parameters had been performed previously.[24–26] The tapes were then laminated via hot pressing at 75 °C. Each sandwich structure comprised porous tape layers laminated between solid (nonporous) tape layers (Fig. 1), with a total of 12 layers for each substrate. Three configurations, skin–core–skin (0-12-0, 1-10-1,

and 2-8-2) were studied, with the numbers representing the number of layers in the skin/core as shown in Table II.

The laminated tapes were then pyrolized to remove the organic additives and the polymer microspheres. The burnout cycle was determined using thermogravimetric analysis, and the optimum heating rate was found to be a slow rate of 0.1 °C/min. Because the microspheres contributed to the volume of organic content, a slower rate was needed to pyrolyze the relatively large amount of organic materials as compared to tapes without microspheres (0.5 °C/min). A faster pyrolysis rate of the microspheres resulted in samples that were warped and had large holes on the surface, as this did not allow the gases to escape and contributed to the formation of cracks and bubbles. The tapes were then reaction sintered in a carbothermal reduction furnace at 1680 °C for 12 h under 0.3 MPa nitrogen to simultaneously achieve conversion and densification.

Density measurements were performed using gas pycnometry (Ultrapycnometer 1000) and compared with porosity measurements using mercury intrusion porosimetry (Autopore III, Micromeritics, GA). The relative density of each composition was calculated from the weighted mean of the theoretical value of each member (AlN, 3.26 $Mg/m^3$; $Al_2O_3$, 3.98 $Mg/m^3$; $Y_2O_3$, 5.03 $Mg/m^3$). Thermal conductivity of the samples was measured using laser flash method (Netzsch LFA427). Thermal expansion coefficient was determined using a dynamic mechanical analyzer (Perkin-Elmer TMA 7e) in nitrogen. The parallel capacitance ($C_p$) and loss tangent (dissipation factor, $D$) of the tapes were obtained at 1 MHz (Hewlett-Packard 4194A impedence/network analyzer), room temperature. Dielectric constant was then calculated. Mechanical properties were measured using the Instron mechanical tester.

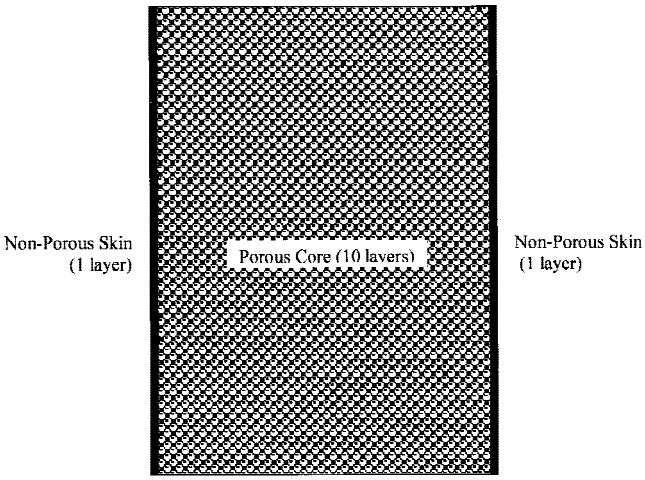


FIG. 1. Schematic diagram of a sandwich substrate, $X_{(1\text{-}10\text{-}1)}$.

TABLE II. Various sandwich structure configurations studied.

| Sample | Skin layer | Core layers | Skin layer | Porous core |
|---|---|---|---|---|
| $0_{(0\text{-}12\text{-}0)}$ | ⋯ | 12 | ⋯ | Nonporous |
| $5_{(0\text{-}12\text{-}0)}$ | ⋯ | 12 | ⋯ | 5 |
| $5_{(1\text{-}10\text{-}1)}$ | 1 | 10 | 1 | 5 |
| $5_{(2\text{-}8\text{-}2)}$ | 2 | 8 | 2 | 5 |
| $10_{(0\text{-}12\text{-}0)}$ | ⋯ | 12 | ⋯ | 10 |
| $10_{(1\text{-}10\text{-}1)}$ | 1 | 10 | 1 | 10 |
| $10_{(2\text{-}8\text{-}2)}$ | 2 | 8 | 2 | 10 |
| $15_{(0\text{-}12\text{-}0)}$ | ⋯ | 12 | ⋯ | 15 |
| $15_{(1\text{-}10\text{-}1)}$ | 1 | 10 | 1 | 15 |
| $15_{(2\text{-}8\text{-}2)}$ | 2 | 8 | 2 | 15 |
| $20_{(0\text{-}12\text{-}0)}$ | ⋯ | 12 | ⋯ | 20 |
| $20_{(1\text{-}10\text{-}1)}$ | 1 | 10 | 1 | 20 |
| $20_{(2\text{-}8\text{-}2)}$ | 2 | 8 | 2 | 20 |

## III. RESULTS AND DISCUSSION

Microstructural observations of fracture surfaces of the green sandwich structures after pyrolysis indicated good homogeneity and pore distribution (Fig. 2). In addition, no delamination or cracking between the porous cores and nonporous skin interfaces was present.

Mercury porosimetry was performed on the nonsandwich substrates to determine pore size and distribution of the tapes, as sintering behavior is dependent on pore size and distribution. The pore-size distribution of various nonsandwich substrates is shown in Fig. 3. Nonporous substrates possessed a unimodal pore-size distribution with an average pore radius of 0.15 μm. Porous substrates had a bimodal pore-size distribution with peaks at 0.15 and 18.1 μm (from added microspheres). Table III presents these results.

Figure 4 shows the scanning electron microscopy (SEM) micrograph of the fracture surface of the sintered nonporous sample, $O_{(0\text{-}12\text{-}0)}$. As observed, sintering was complete with pore closure of the small pores and

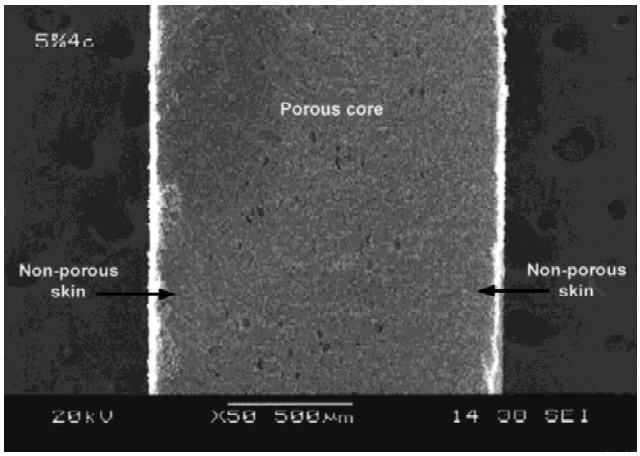


FIG. 2. SEM micrograph of a typical fracture surface of green sandwich substrate.

uniform grain growth. The converted AlN grains exhibited a well-defined morphology, having a fully dense contiguous microstructure. The sintering additive $Y_2O_3$ reacted to form YAG, while there was about 2–3% residual nonconverted $Al_2O_3$ (Fig. 5). For samples with the added porosity via microspheres, the fracture surface clearly shows nice spherical isolated pores (Figs. 6 and 7). It is believed that this was due to a higher diffusion rate and lower activation energy for grain growth in the presence of the liquid phase containing an oxide with a lower melting temperature. Atom movement necessary for pore movement was concentrated along the grain boundaries or triple points of the AlN grains. This sintering aid effectively lowered the surface tension of the matrix in the grain boundary zones. The atom mobility was increased, thus facilitating movement of the smaller pores toward the surface and out of the sintering matrix. In the final stage of sintering, densification occurs by the removal of closed pores by grain growth in the presence of the liquid phase. As for the larger added pores, the matrix grains collected around them and sintered smaller. The average pore size of the sintered body reduced from 18.1 to 16.6 μm. This was due to the lower contact angle between the solid grains and liquid phase, thus allowing the liquid to make contact with or wet the solid grains more readily, enhancing grain growth and reducing pore size. However, the added porosity did not seem to have any influence on grain size.

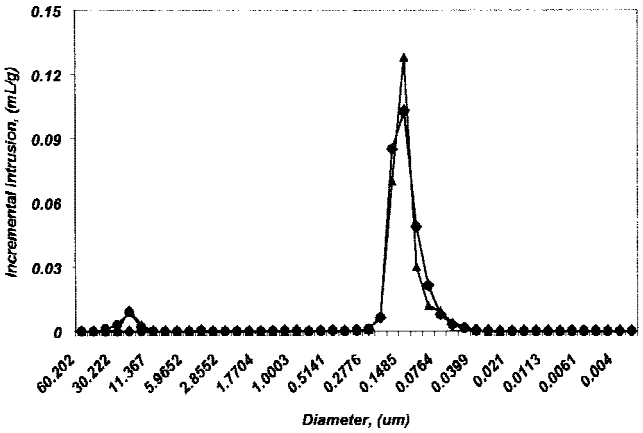


FIG. 3. Mercury porosimetry of nonsandwich substrates (♦, 0%; ●, 10%, ▲, 20%).

TABLE III. Mercury porosimetry results of nonsandwich substrates.

| Sample | Added porosity (vol%) | Average pore diameter (μm) | Bulk density (g/mL) | Apparent density (g/mL) | Porosity (%) |
|---|---|---|---|---|---|
| $0_{(0\text{-}12\text{-}0)}$ | 0 | 0.15 | 1.60 | 2.36 | 32.2 |
| $10_{(0\text{-}12\text{-}0)}$ | 10 | 0.49 | 1.59 | 2.53 | 37.1 |
| $20_{(0\text{-}12\text{-}0)}$ | 20 | 0.93 | 1.58 | 2.71 | 41.9 |

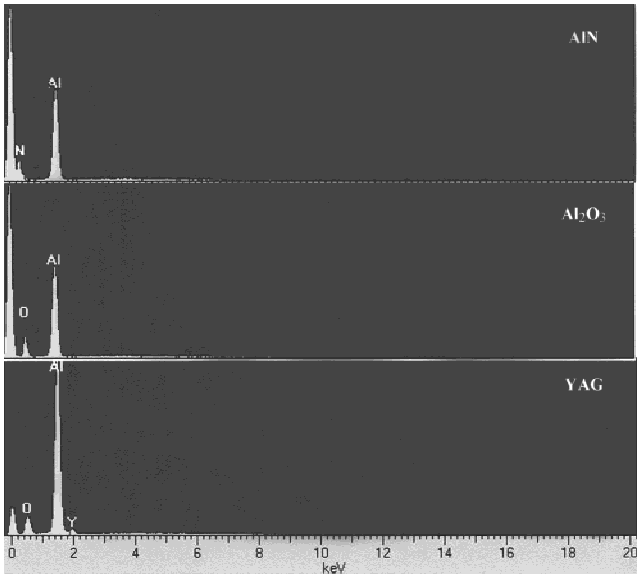


FIG. 5. EDX spectra of different phases as indicated in Fig. 4.

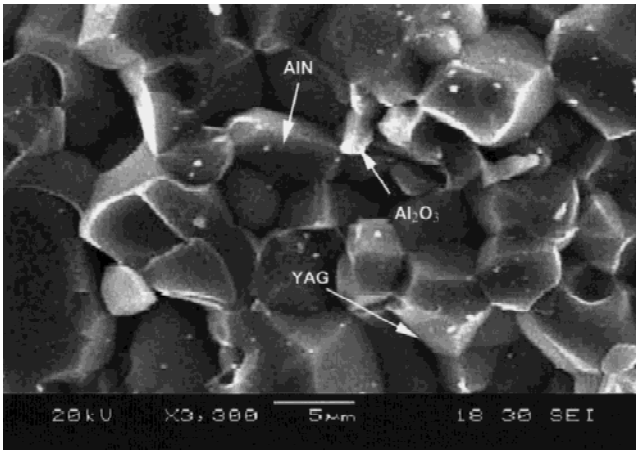


FIG. 4. SEM micrograph of a fully sintered nonporous AlN substrate.

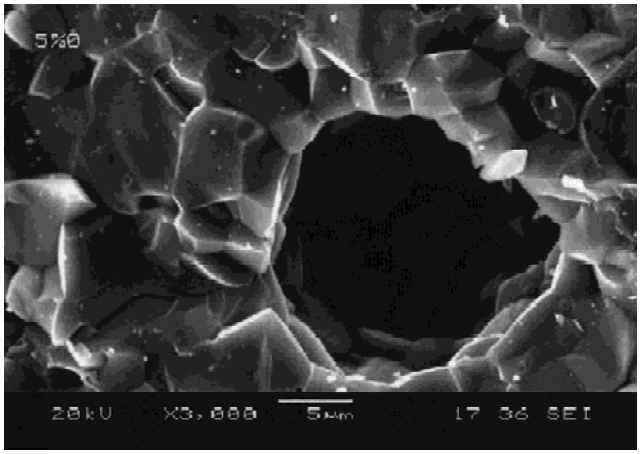


FIG. 6. SEM micrograph of a single isolated pore.

The AlN content in the porous tapes was about 2% higher than that of nonporous converted tapes, and this could be attributed to the nitrogen gas filling up the open pores during reaction sintering and allowing for a greater conversion due to proximity.

Figure 8 shows sandwich substrate sintered samples $10_{(0\text{-}12\text{-}0)}$, $10_{(1\text{-}10\text{-}1)}$, and $10_{(2\text{-}8\text{-}2)}$, all having 10% added porosity but different numbers of skin layers. No interfacial cracking or delamination was observed between the various porous core and nonporous skin layers.

Table IV summarizes the various properties of the samples.

Figure 9 shows the effect of microspheres addition on relative density. As observed, higher volumes of added microspheres resulted in lower densities, showing a linear trend. In addition, due to the lower porosity in the skin layers, substrates with more skin layers had higher density values. This in turn influenced the dielectric constant, thermal conductivity, and mechanical strength.

Figure 10 shows the graph of dielectric constant against porosity. As expected, dielectric constant was decreased with increasing porosity values. The lowest dielectric constant value achieved was about 4.1, in the substrate having 20 vol% added microspheres and a porosity of 15.3%. The loss tangents were reasonably low for all samples. While no systematic correlation was observed in losses. At high frequency, polarization was dominated by electronic polarization, and the loss was mainly attributed to phonon scattering. Mackrodt *et al.*[27] have shown that the presence of a free surface (such as a pore) led to the relaxation of the crystal lattice. This relaxed surface was effectively a different structure as the bulk material, and could be considered a large defect area. This would increase dielectric loss.

Figure 11 shows the graph of thermal conductivity against porosity for the various samples. Previous works[28,29] have shown that the thermal conductivity of polycrystalline AlN bodies having a porosity of more than 2% is influenced mainly by its porosity, whereas thermal conductivity of bodies having a porosity of less than 2% are influenced by the nature of its secondary phase. This trend was also observed in Fig. 11. For samples having less than 2% porosity, the thermalconductivity was seen to decrease significantly with the same increases in porosity. After the 2% mark, the grain boundary effects were less significant and reduced the

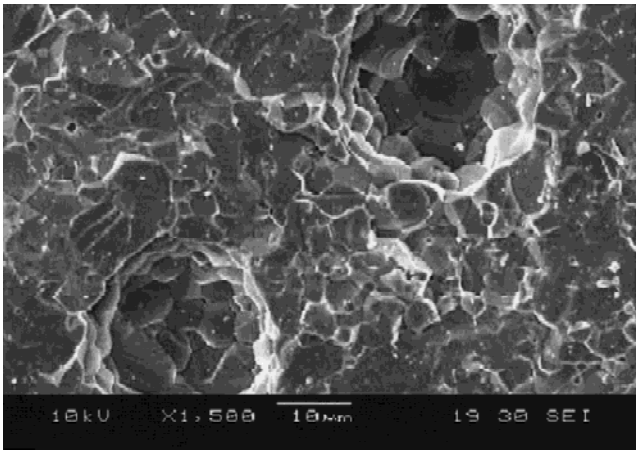


FIG. 7. SEM micrograph of noninterconnected pores.

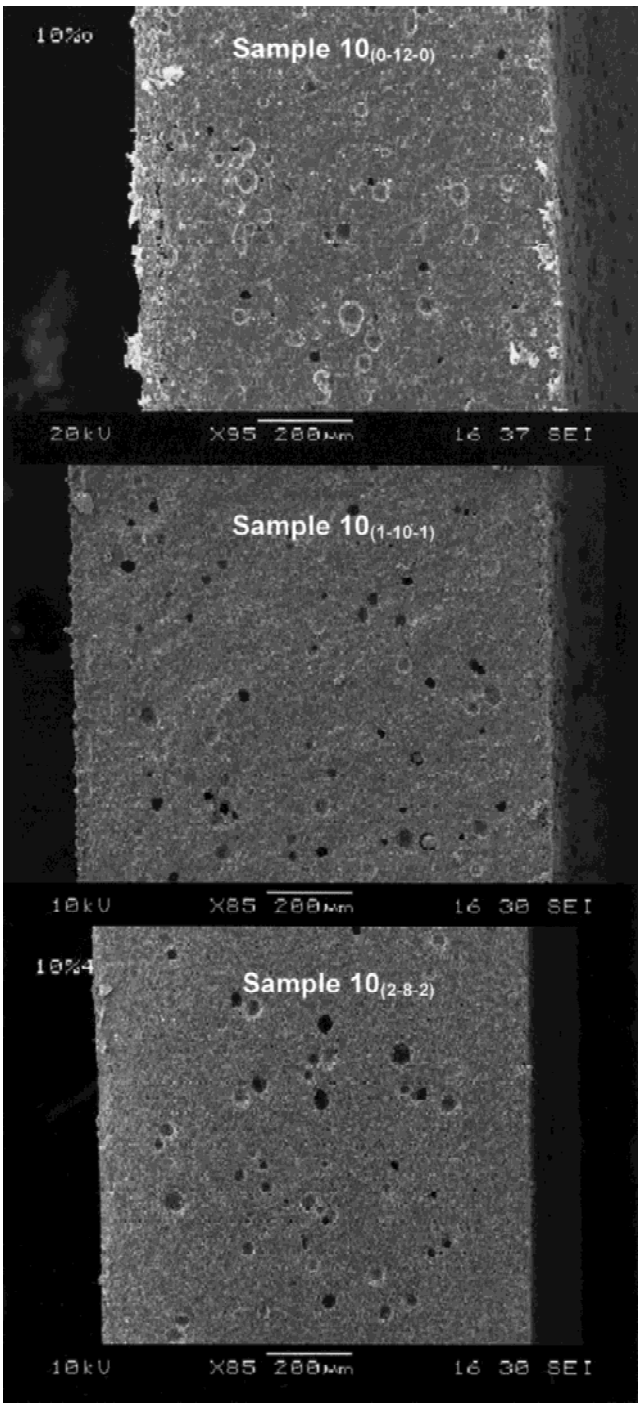


FIG. 8. SEM of a sintered sandwich substrate.

rate of decrease in thermal conductivity. This portion of the curve adhered to commonly used models using a first-order approximation to an exponential form.[29] As observed in Fig. 12, the presence of the solid layer skins did help to improve thermal conductivity values, in addition to improving mechanical strength. It was also observed that with an increasing porosity value for the core, the presence of the skin had little effect on thermal conductivity.

Figure 13 shows the thermal expansion coefficient (CTE) values for the various substrates. For microelectronics substrate applications, the CTE value of the substrate between 30 and 300 °C is important. Since the CTE of AlN is similar to that of silicon, this is desirable in the prevention of thermal mismatch and cracking. CTE values depend mostly on the phase composition of the substrate, and porosity does not influence the values of CTE in bulk materials. This was also observed in the sandwich substrates, and no trend was observed here. CTE values had an average of $4.12 \times 10^{-6}$/ °C with a standard deviation of $0.1 \times 10^{-6}$/ °C.

Symmetrical stacking was used in the sandwich substrates as this prevented distortion and local microstructural damage/failure, because the coupling forces largely cancel each other out due to the property difference.[30] Figure 14 shows the graph of flexure strength against porosity for the various substrates. The flexure strength decreased with increases in porosity, although the trend

TABLE IV. Properties of the various sandwich substrates.

| Parameter | Samples (Microspheres vol%) | | | | | | | | | | | | |
|---|---|---|---|---|---|---|---|---|---|---|---|---|---|
| | 0 | 5 | 5 | 5 | 10 | 10 | 10 | 15 | 15 | 15 | 20 | 20 | 20 |
| Configuration | 0-12-0 | 0-12-0 | 1-10-1 | 2-8-2 | 0-12-0 | 1-10-1 | 2-8-2 | 0-12-0 | 1-10-1 | 2-8-2 | 0-12-0 | 1-10-1 | 2-8-2 |
| Relative density (%) | 99.0 | 97.2 | 97.8 | 98.6 | 93.7 | 94.9 | 96.0 | 89.1 | 89.9 | 91.0 | 84.7 | 85.6 | 86.0 |
| Dielectric constant | 8.2 | 7.9 | 8.0 | 8.1 | 6.0 | 7.0 | 7.2 | 5.1 | 5.0 | 5.3 | 4.6 | 4.2 | 4.1 |
| Thermal conductivity (W/mk) | 86.8 | 52.1 | 55.8 | 65.6 | 23 | 30.2 | 47.1 | 11.3 | 11.4 | 13.1 | 9.5 | 9.8 | 10.4 |
| CTE (ppm/°C) | 4.17 | 4.02 | 4.21 | 4.12 | 4.26 | 3.98 | 4.00 | 4.09 | 4.22 | 4.15 | 4.14 | 4.24 | 4.00 |
| Young's modulus (GPa) | 290 | 240 | 260 | 278 | 232 | 251 | 266 | 186 | 202 | 231 | 166 | 171 | 183 |
| Porosity (%) | 1.0 | 2.8 | 2.2 | 1.4 | 6.3 | 5.1 | 4.0 | 10.9 | 10.1 | 9.0 | 15.3 | 14.4 | 14.0 |

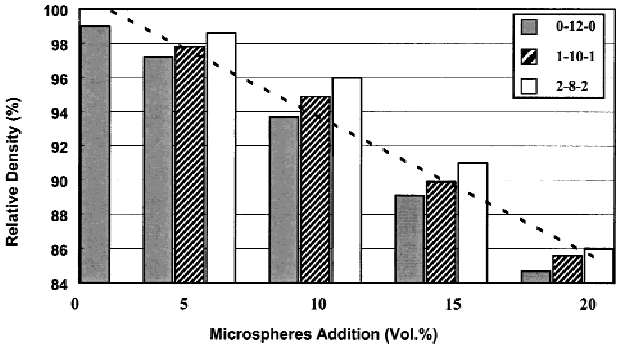


FIG. 9. Effect of microspheres addition on relative density.

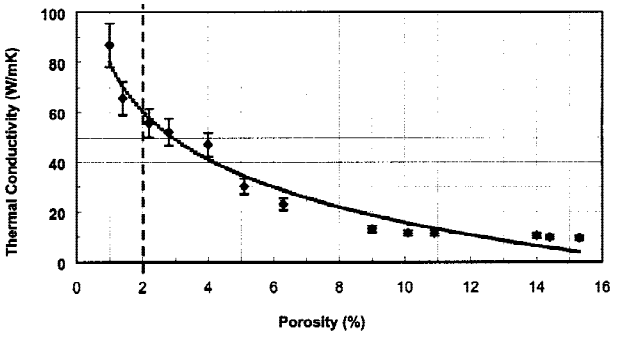


FIG. 11. Graph of thermal conductivity against porosity.

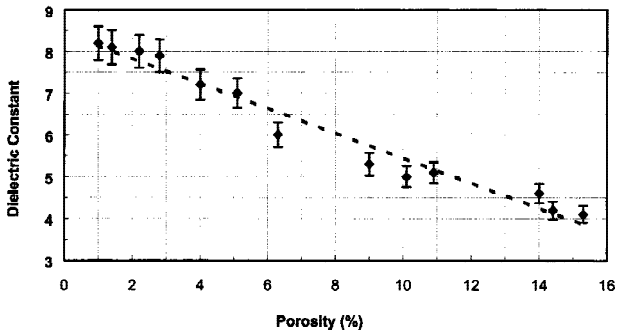


FIG. 10. Graph of dielectric constant against porosity.

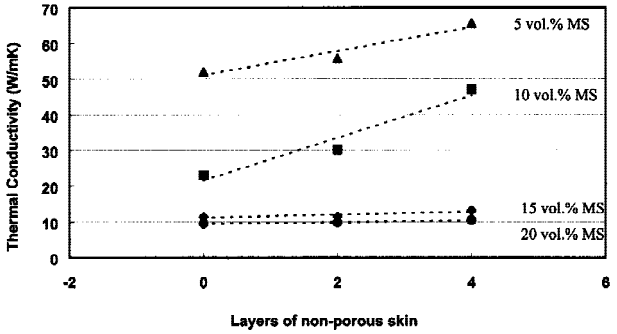


FIG. 12. Thermal conductivity dependence on nonporous skin layer.

was not linear. This trend was found to be similar to the Ryshkewich expression,[31,32] which explains strength–porosity relationships. The expression is given as

$$S = S_0 e^{-bP} \quad , \tag{2}$$

where $S$ and $S_0$ are the strengths for the porous and dense bodies, respectively, $P$ is the volume fraction, and $b$ is an empirical constant relating porosity to mechanical strength, a lower value representing higher strength. Porous substrates produced by incomplete sintering results in the pores having a sharp re-entrant angle, and this empirical constant, $b$, is typically 7 for these partially sintered substrates. For the sandwich substrates, as the added pores were spherical, the matrix crack stress was distributed evenly around the pores and avoided the extreme stress concentration typically found in sharp angles; hence, the constant, $b$, was significantly lower at 4.76. In addition, as the pores were noninterconnected, this increased the crack propagation distance, therefore effectively slowing crack growth. As the mode of failure was typically tensile failure of the skin, this stronger nonporous skin improved the strength-to-weight ratio of the sandwich substrate. Figure 15 presents Young's modulus values for the various substrates. Increasing porosity values decreased Young's modulus, while an increasing number of skin layers improved Young's modulus.

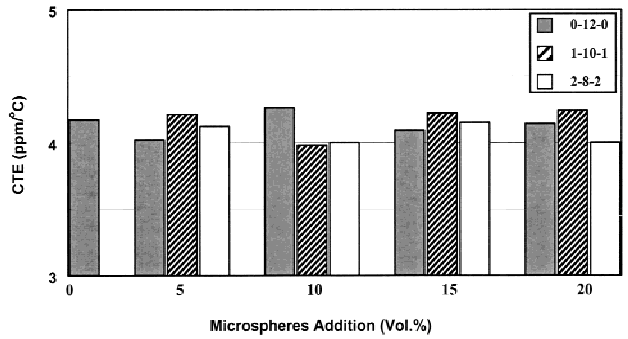


FIG. 13. CTE for different sandwich substrates.

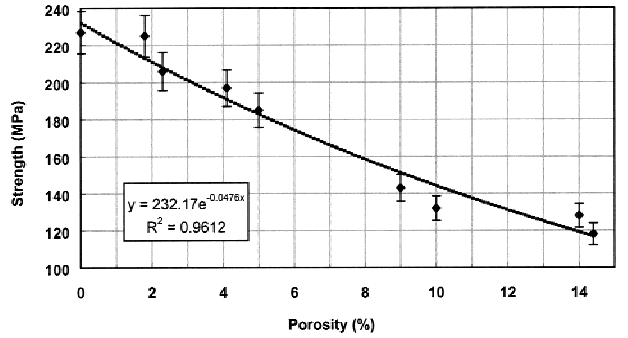


FIG. 14. Graph of flexure strength against porosity.

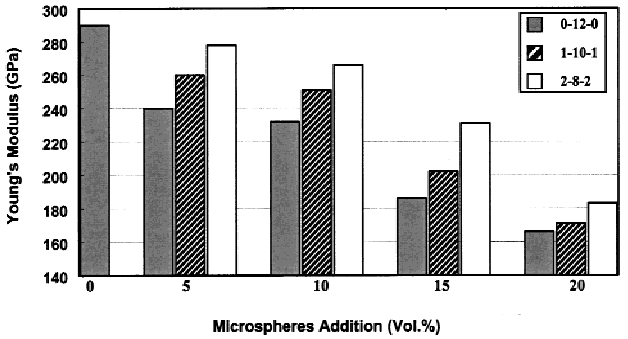


FIG. 15. Young's modulus of the various sandwich substrates.

## IV. CONCLUSION

AlN multilayered sandwich substrate comprising porous tape-cast layers sandwiched between nonporous layers were fabricated. No interface cracking or delamination was observed in the substrates as a result of the processing. The added porosity resulted in a decrease in the substrate dielectric constant in correspondence to porosity volume. Mechanical strength of the sandwich substrates was improved over that of nonsandwich porous substrates, while substrates having noninterconnected pores showed higher mechanical strength than substrates with connected pores. Substrates with more than 2% porosity showed porosity-dependent thermal conductivity values, while thermal conductivity of substrates with less than 2% porosity was dependent on grain boundary effects. The thermal expansion coefficient of the substrates was unaffected by porosity levels.

## REFERENCES

1. Semiconductor Industry Association, International Technology Roadmap for semiconductors, ITRS Report 1999 Edition (1999).
2. R.C. Buchanan, *Ceramic Materials for Electronics: Processing, Properties and Applications* (Marcell Decker Inc., New York, 1986).
3. J.S. Reed, *Principles of Ceramics Processing* (John Wiley & Sons, New York, 1994).
4. B. Schwartz, Am. Ceram. Soc. Bull. **65**(7), 1032–1035 (1986).
5. T. Chartier and E. Streicher, J. Eur. Ceram. Soc. **9,** 231–242 (1992).
6. J.M. Haussone, Mater. Manuf. Processes **10**(4), 717–755 (1995).
7. D. Wirth, *Engineered Materials Handbook* (ASTM, West Conshohocken, PA, 1991), Vol. 4 pp. 1107–1111.
8. J.P. Disson and R. Bachelard, Ind. Ceram. **896**(9), 602–606.
9. W.T. Shugg, *Handbook of Electrical and Electronic Insulating Materials,* 2nd ed. (IEEE, Piscataway, NJ, 1995).
10. A.A. Mohammed and S.J. Corbert, Proc. Int. Symp. Microelectron. 218–224 (1985).
11. G. Selvaduray and L. Sheet, Mater. Sci. Technol. **9,** 463–473 (1993).

12. F. Boey, L. Cao, K.A. Khor, and A.I.Y. Tok. Acta Mater. (in press).
13. F.Y.C. Boey, X.L. Song, Z. Gu, and A.I.Y. Tok, J. Mater. Process. Technol. **89–90,** 478–480 (1999).
14. D.W. Kellerman, in *Hollow and Solid Spheres and Microspheres: Science and Technology Associated with Their Fabrication and Application* (Mat. Res. Soc. Symp. Proc. **372,** Pittsburgh, PA, 1995). pp. 239–245.
15. E.H. Kraft, *Materials and Designs for Advanced MIC Packages* (American Institute of Physics, Melville, NY, 1986), pp. 255–266.
16. A.I.Y. Tok, F.Y.C. Boey, and W.J. Clegg, J. Mat. Res. (2001, in press).
17. G. Carprino and A. Langella, J. Comp. Mater. **34**(9), 791–814 (2000).
18. D.J. Bakos and G.C. Papanicolaou, Comp. Sci. Technol. **49,** 35–43 (1993).
19. B. Lamy and E. Dixneuf, J. Mater. Sci. Lett. **18,** 607–608 (1999).
20. Y. Shenbar, Y. Prostig and E. Altus, Comp. Struct. **35,** 143–152 (1995).
21. G. Caprino and R. Teti, *Sandwich Structures Handbook* (Prato Publications, Prato, Italy, 1989).
22. M. Vincenzo, P. Sglavo, P. Bosceri, E. Trentini, and M. Ceschini, J. Am. Ceram. Soc. **82**(8), 2269–2272 (1999).
23. Y. Huang, Development of hollow polymer microspheres, Master of Engineering Thesis, Nanyang Technological University, Singapore (1999).
24. A.I.Y. Tok, F.Y.C. Boey, and Y.C. Lam, Mater. Sci. Eng. **A280,** 282–288 (2000).
25. A.I.Y. Tok, F.Y.C. Boey, and K.A. Khor, J. Mater. Process. Technol. **89–90,** 508–512 (1999).
26. S.C. Joshi, Y.C. Lam, F.Y.C. Boey, and A.I.Y. Tok, J. Mater. Process. Technol. (2001).
27. W.C. Mackrodt, in *Advances in Ceramics*, edited by C.R.A. Cadow and E.C. Mackrodt (American Ceramic Society, Westerville, OH, 1987) pp. 293–306.
28. J.H. Enloe, R.W. Rice, J.W. Lau, R. Kumar, and S.Y. Lee, J. Am. Ceram. Soc. **74**(9), 2214–2219 (1991).
29. N. Kuramoto, H. Taniguchi and I. Aso, Am. Ceram. Soc. Bull. **68**(4), 833–837 (1989).
30. D. Hill and T.W. Clyne, *An Introduction to Composite Materials*, 2nd ed. (Cambridge University Press, Cambridge, United Kingdom, 1996).
31. E. Ryahkewich, J. Am. Ceram. Soc. **36**(2), 65–68 (1953).
32. W. Duckworth, J. Am. Ceram. Soc. **36**(2), 69 (1953).